Joint CSCE Construction Specialty & CRC Conference 2025
Conférence conjointe spécialisée en construction de la SCGC et CRC-2025

Montreal, Quebec
July 28-31, 2025 / *28-31 juillet 2025*

ENHANCING FALL RISK ASSESSMENT BY MONITORING PHYSICAL AND PHYSIOLOGICAL RESPONSE THROUGH WEARABLE INERTIAL MEASUREMENT UNIT AND ELECTRODERMAL ACTIVITY SENSORS

H. Lee[1], J. Sohn[2], J.V. Jacobs[3], and S. Lee[2]*

[1] School of Project Management, University of Sydney, Sydney, NSW, Australia
[2] Department of Civil and Environmental Engineering, University of Michigan, Ann Arbor, MI, USA
[3] Risk Control Services, Liberty Mutual Insurance, Boston, MA, USA

ABSTRACT: Falls are the leading cause of unintentional injury, threatening public health and safety. Assessing how individuals perceive and respond to fall hazard exposure is essential to mitigate their fall risks. Wearable inertial measurement unit (IMU) sensors have been used to monitor abnormal body movements, such as loss of balance, caused by fall hazard exposure. The abnormality of IMU data is quantified into a fall hazard index, which represents the level of hazard exposure. However, relying solely on physical body responses often overlooks individual differences in perceiving and responding to fall hazards. To address this limitation, this study integrates electrodermal activity (EDA) data to measure physiological responses and refine the fall hazard index derived from IMU data. To test how the refined fall hazard index better represents fall risk perception, a total of 60 subjects participated in a 750-meter predetermined route trial with different types of fall hazards. After the trial, subjects rated the perceived risk of falls for each hazard on a 1 to 5 scale (1 = low risk, 5 = high risk). Spearman's rank correlation was used to statistically determine whether the fall risk perception correlated with the fall hazard index. The refined fall hazard index showed a stronger correlation with perceived fall risks (correlation coefficient = 0.82, p-value < 0.01) compared to the IMU-based fall hazard index (correlation coefficient = 0.60, p-value < 0.01). This study highlights the robustness of combining wearable IMU and EDA sensors for individual fall risk assessment, establishing a foundation for broader implementation.

1. INTRODUCTION

Slip, Trip, and Fall (STF) hazards are the leading cause of unintentional fatalities and resulted in approximately 9.7 million emergency room visits and over 180 billion dollars in medical expenses (Centers for Disease Control and Prevention (CDC) 2022). In addition, workplace same-level falls represent the third-ranked most costly causes of serious, non-fatal injuries in the construction industry (2024 Liberty Mutual Workplace Safety Index). To reduce fall-related accidents, it is imperative to identify worksite STF hazards to enable proactive intervention before fall incidents occur. When people are exposed to STF hazards, they often lose their balance, exhibiting abnormal body movements that differ from normal walking patterns. Repeated exposure to such STF hazards can significantly increase fall risk. Individual fall risk assessment has been based on monitoring physical body movements (Antwi-Afari and Li 2018; Okunola et al. 2024; Pang et al. 2019). Wearable inertial measurement unit (IMU) sensors have been widely used to monitor physical body movements effectively (Pang et al. 2019). These sensors can be attached to various body parts (e.g., the wrist, hip, or ankle) and capture 3-axis linear acceleration and angular velocity data based on the body part movements (Zhao and Obonyo 2020).

Previous studies have focused on differentiating the characteristics of IMU data (e.g., statistical values or temporal patterns) that were collected during exposure to STF hazards and normal walking. Threshold-based and machine learning-based models have been the primary approaches to detect abnormal IMU data during walking (Pang et al. 2019; Ramachandran and Karuppiah 2020). While these approaches assess the frequency of exposure to STF hazards, they do not quantify the extent of exposure, which is a critical factor in fall risk assessment. Our previous study (Lee et al. under review) scored IMU data abnormality to a range from 0 to 1, where higher values correspond to greater movement abnormality. This normalized abnormality score was used as a fall hazard index. This study demonstrated that the fall hazard index aligned with fall hazard perception on a 1 to 5 scale, where 1 represented 'low risk' and 5 represented 'high risk,' suggesting that the fall hazard index could serve as a reliable indicator of fall risk.

Useful fall hazard assessment should strongly correlate with a person's perceived fall risk, which is influenced by physiological responses as well as physical body movements. For example, loss of balance also increases physiological arousal (Sibley et al. 2014). Our previous study (Sohn et al. 2024) monitored physiological arousal using a wearable electrodermal activity (EDA) sensor and demonstrated the feasibility of analyzing EDA data to distinguish STF hazard exposure from other walking activities. However, it remains unclear how to effectively integrate physiological arousal monitoring with IMU-based fall risk assessment. This study proposes an approach to enhance the IMU-based fall hazard index by incorporating EDA data, aiming for a more robust and perception-aligned fall hazard assessment.

2. IMU-BASED FALL RISK ASSESSMENT

Traditional IMU-based fall risk assessment detects singular anomalous data points in sequential IMU data. This approach predetermines a threshold for IMU data, representing the maximum allowable value during normal walking (Karel et al. 2010; Lee et al. 2015; Weiss et al. 2010). Any data point exceeding the threshold value is detected as STF hazard exposure. Although a single axis of IMU data can be analyzed, a combined value derived from 3-axis IMU data—calculated using the first differences and first derivatives of the sum of 3-axis acceleration data—is generally used, as it enhances the detection of abnormal body movements caused by STF hazard exposure. Threshold-based models are prevalent as they provide a simple method with low computational costs. In addition, machine learning algorithms have been employed for detecting abnormal patterns of IMU data. A previous study (Albert et al. 2012) applied traditional machine learning algorithms for fall risk assessment, such as decision trees (DT), k-nearest neighbors (kNN), Naïve Bayes (NB), sparse multinomial logistic regression (SMLR), and support vector machine (SVM). Deep learning algorithms were also applied for fall risk assessment, including recurrent neural network (RNN), long short-term memory (LSTM), and transformer. These algorithms have provided higher performance compared to traditional machine learning algorithms because deep learning algorithms better capture complex temporal patterns in the sequential IMU data (Lee et al. 2022).

However, even with advanced models, solely relying on IMU data is prone to yield false positives due to natural walking variability. For example, abruptly starting to walk after a brief pause, shifting body posture during walking, or changing in walking direction may produce abnormal patterns of IMU data that are not related to actual STF hazard exposure. Our previous study (Sohn et al. 2024) demonstrated that physiological arousal measured via wearable EDA sensors could statistically differentiate among STF hazard exposure, normal walking, and transitional walking—such as bending, hopping, and ankle rotation. Unlike normal walking, both STF hazard exposure and transitional walking generate spikes in IMU data, making it difficult to distinguish them based on IMU data alone. However, the EDA data showed significantly higher arousal levels following STF hazard exposure, indicating its potential as a discriminative factor. Because EDA reflects the individual's internal response to perceived risk or postural instability, it provides complementary information that is not captured by IMU data alone. While our prior work highlights the feasibility of using physiological signals to distinguish STF hazard exposure from walking variations, the potential benefit of integrating EDA with IMU data to enhance fall risk assessment remains underexplored. In this context, this study aims to enhance the accuracy and reliability of IMU-based fall risk assessment by integrating physiological arousal data from EDA sensors. By combining IMU and EDA data, the authors

propose a comprehensive fall hazard index that more accurately reflects individual perceptions of fall risk, enabling the precise identification of high-risk hazards and supporting preventative interventions before fall incidents occur.

3. METHOD

3.1 Subjects

A total of 60 subjects participated, ranging in age from 20 to 70 years. None reported any clinical conditions that could impact their physical or mental capacity for daily walking. During recruitment, individuals with a history of traumatic STF hazard exposure were excluded to avoid potential atypical physical and physiological responses that could influence the results. This study was approved by the Institutional Review Board at the University of Michigan (HUM00220842).

3.2 Protocol

First, we placed a wearable IMU (i.e., MetaMotionS) and EDA (i.e., Empatica E4) sensor on each subject's wrist during data collection. The sensor location on the wrist plays a critical role in fall risk assessment. When individuals are exposed to STF hazards, they often experience a loss of balance and initiate corrective responses to regain stability. A wrist-worn IMU sensor effectively captures abnormal arm movements in response to balance disturbances. Although IMU and EDA data were captured separately in this study, integrating these two sensing modalities into a single wrist-worn device in future applications could significantly enhance the practical applicability of fall risk assessments. IMU data was recorded at a 60-Hz sampling rate, while EDA data was recorded at a 4-Hz sampling rate. Each subject walked naturally along a 750-meter predetermined route at the University of Michigan North Campus, where they were exposed to three different STF hazards: debris, uneven surfaces, and slippery surfaces (see Figure 1). The route was designed to vary both the difficulty level and exposure time for each hazard. Debris was created by scattering tree branches on the walkway. Uneven surfaces consisted of naturally existing gravel layers on the route. Slippery surfaces were simulated using a water-saturated steel plate. Subjects traversed the uneven surface in at least 10 steps, while the debris and slippery surfaces were set to 5-7 steps. After data collection, each subject completed a survey using a five-point numeric scale to evaluate their perceived fall risk for each hazard exposure. Subjects rated the level of fall risk associated with each hazard exposure from 1 to 5, where 1 indicated 'low risk' and 5 indicated 'high risk.' This self-reported score was then compared with the fall hazard index.

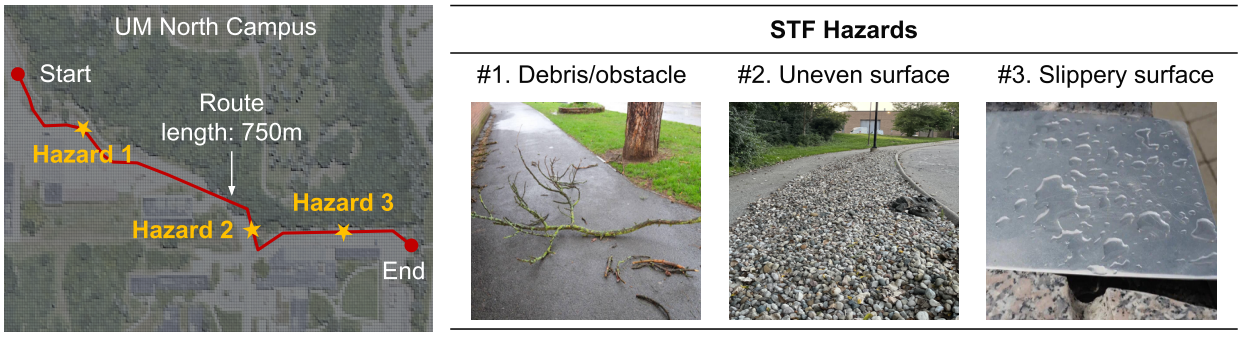

Figure 1: Predetermined route with locations and types of STF hazards.

3.3 Data Processing

Our previous study (Lee et al. under review) developed an unsupervised model for IMU-based fall risk assessment, generating a fall hazard index based on IMU data abnormality. This current study refines the model by integrating EDA data, which monitors physiological arousal, to improve correlation with individual

perceived fall risk. First, we summarize the unsupervised IMU-based fall risk assessment model and then explain the integration of EDA data into the model.

3.3.1 IMU-based Fall Risk Assessment Model

This study used the mediolateral axis of angular velocity data, which captures repetitive side-to-side arm movements during walking. The overall assessment process is as follows: The IMU data were segmented into 2-second subsequences, which were transformed using local convolution and reduced via PCA. The transformed data were projected into a 2D space to identify pattern clusters, then converted into a graph structure where nodes represented subsequences and edges represented transitions between two subsequences. A fall hazard index was calculated based on graph metrics. The phasic component of the EDA signal was then extracted, normalized, and temporally aligned with the IMU data. Finally, the refined fall risk index was obtained by multiplying the IMU-based score and the EDA value.

The time-series data was first transformed into a 2-dimensional space, where similar subsequences cluster together while abnormal subsequences remain isolated geometrically. For transformation, a moving window of 2 seconds (120 data points) was used to sample subsequences from the data, where the window length was empirically determined to capture abnormal patterns of IMU data due to fall-hazard exposure. The subsequences are then mapped into a 3-dimensional space. First, local convolution was applied using a moving window with a 40-data-point length, which extracts localized pattern changes around each data point. Local convolution created a multi-dimensional convolution space, where the size of dimensions corresponds to 81 local convolution steps multiplied by the number of subsequences, which depends on the total IMU data length. Principal component analysis (PCA) is then used to reduce this high-dimensional space into a 3-dimensional space (Ux, Uy, and Uz). To align the Uz axis with a temporal perspective, the space is rotated, where all data points fluctuate between the minimum and maximum values along the Uz axis. Finally, the rotated 3-dimensional space is projected onto the Uz axis to create a 2-dimensional space. As shown in Figure 2, subsequences T1 and T2 exhibit similar patterns and are positioned close to each other, whereas T3, which deviates from the pattern, remains relatively isolated.

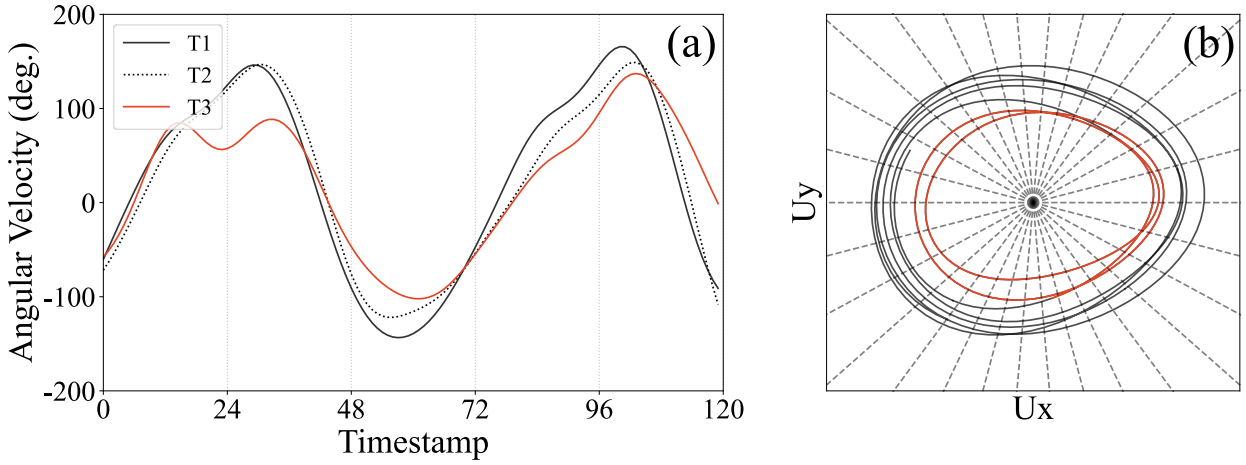

Figure 2: Data transformation from walking subsequences (a) to 2-dimensional space (b) for similarity analysis.

Graph-structured data consists of nodes and edges, such that nodes represent the number of clustered subsequences within a specific section in the 2-dimensional space, and edges define the relationships between nodes. Figure 2(b) shows that the space is divided into 30 sections (dashed lines). Nodes are generated by counting the intersections between subsequences and these dashed lines. Clusters of similar patterns produce denser intersections, while isolated subsequences generate fewer intersections. As shown in Figure 3, local maxima within the intersection distribution are identified as nodes, which are then connected by edges. Each node degree represents the number of connected nodes and edge weights quantify the number of subsequences passing through a given node pair. For example, node N_3 has a

degree of 2, as it is connected to N_1 and N_2. Similarly, E_2 has a weight of 4, indicating that four subsequences pass through the node pair (N_1 and N_3). This process transforms time-series IMU data into graph-structured data.

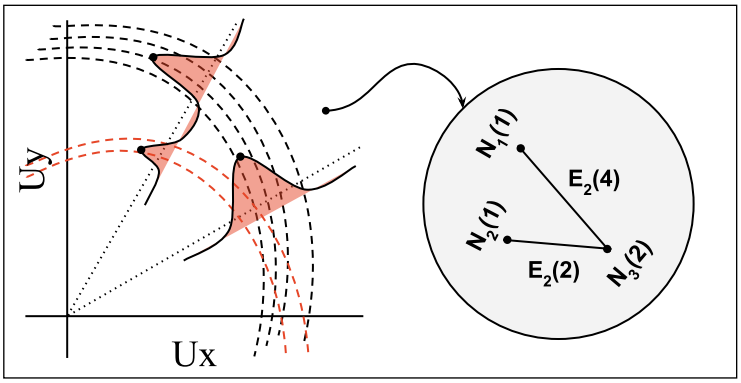

Figure 3: Graph construction: nodes represent IMU subsequences and edges indicate pattern similarity.

For each subsequence, an abnormality score is computed using Equation 1.

[1] $$\sum_{j=i}^{i+l-1} \frac{w(N_j,N_{j+1})deg(N_j-1)}{l}$$

where, $w(N_j, N_{j+1})$: Edge weight; $deg\ (N_j)$: Node degree; i: ith subsequence; and l: Subsequence length

For a given sequence of IMU data, the normality scores of all subsequences are reversed and normalized to range from 0 to 1, where higher values indicate greater abnormality. This abnormality score serves as the fall hazard index. Figure 4 shows time-series IMU data and its fall hazard index, where abnormal patterns are observed between data points 3000 and 4000. During this interval, the fall hazard index exhibits relatively higher values, indicating an increased fall risk.

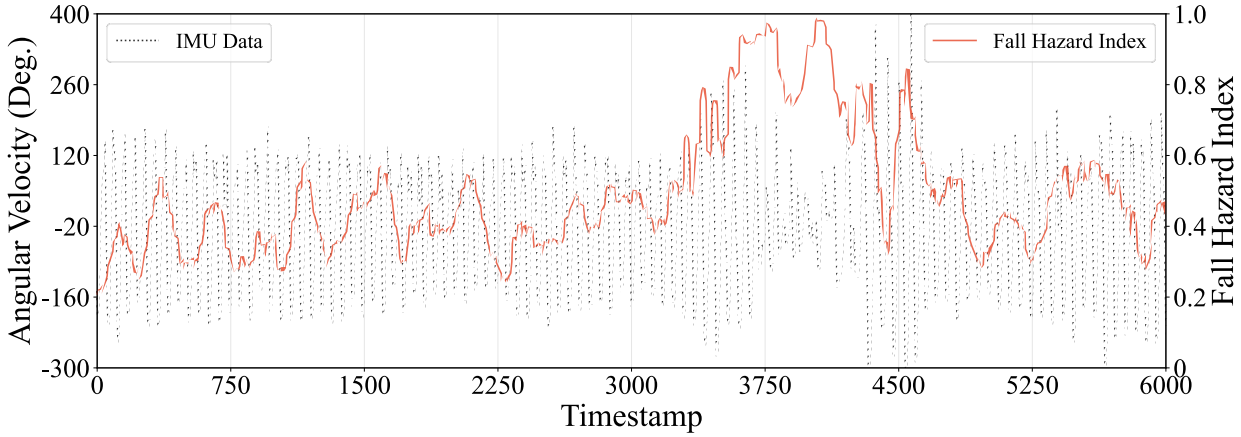

Figure 4: Comparison of raw IMU data and computed fall hazard index highlighting abnormal body movements.

3.3.2 Integration of EDA Data

Raw EDA signals comprise two distinct components: the electrodermal level (EDL) and electrodermal response (EDR). In this study, EDR is utilized to measure physiological arousal changes, as it captures rapid and transient fluctuations in electrical conductance triggered by stressful stimuli, such as STF hazard exposure. To extract EDR, the raw EDA signal is decomposed using a convex optimization-based approach, which effectively separates phasic components from the baseline signal. Then, outliers, caused

by electronic interference and environmental noise, are removed. Finally, EDR values are normalized to a range of 0 to 1 before being integrated with the fall hazard index. The fall hazard index is downsampled to match the sampling rate of the EDA data (4 Hz).

As both IMU-based fall hazard index and the normalized EDA range from 0 to 1, their product also falls within this range, where higher values (close to 1) indicate abnormal patterns in both physical and physiological responses, and lower values (close to 0) reflect normal patterns in both responses. However, a key challenge in integrating these two indices is temporal misalignment, as physical response is typically immediate, whereas physiological response appears more gradually. Specifically, EDA signals exhibit a delayed response of up to 10 seconds compared to IMU signals. To address this, if a peak in the EDA data is detected within a 10-second window corresponding to a peak in the IMU-based fall hazard index, the EDA data is temporally shifted to align with the corresponding peak in the fall hazard index. Compared to the IMU-based fall hazard index shown in Figure 4, which fluctuates between 0.2 and 0.6 even during normal walking patterns, Figure 5 shows the refined fall hazard index—integrated with EDA data—and demonstrates significantly higher values exclusively during STF hazard exposure. This integration results in a clearer distinction between normal walking and STF hazard exposure.

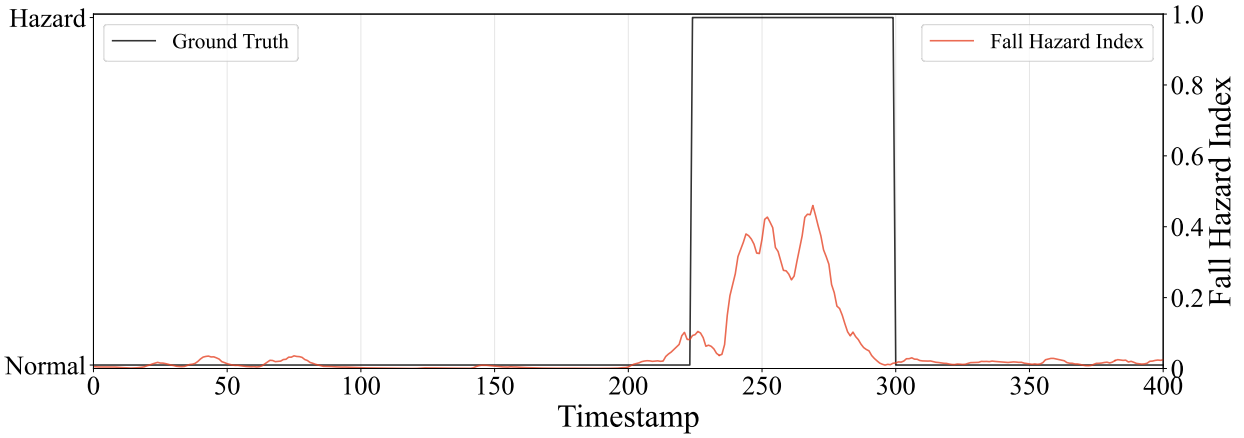

Figure 5: Fall hazard index refined with EDA data, improving the distinction between STF hazard exposure and normal walking variation.

3.4 Statistical Analysis

A Spearman's rank correlation analysis was conducted to statistically validate the correspondence between the fall hazard index and perceived fall risk. This analysis assessed the relationship between the mean differences in fall hazard index values during hazard exposure and normal walking, and the subjects' self-reported fall risk ratings for each hazard exposure. Table 1 presents the ranking results for an exemplar subject. The mean difference in the fall hazard index between hazard exposure and normal walking is 0.92 for uneven surface, 0.72 for debris, and 0.06 for slippery surface. Based on these values, the ranking order derived from the fall hazard index is as follows: uneven surface (1st), debris (2nd), and slippery surface (3rd). In comparison, the self-reported fall risk rankings are 5 for both uneven surface and debris, and 3 for slippery surface. Thus, the ranking order based on perceived fall risk is: uneven surface and debris (tied for 1st) and slippery surface (3rd). By quantifying the degree to which the rankings of the computed fall risk index align with the rankings of self-reported fall risk scores, this correlation analysis provides a robust validation of the fall hazard index's effectiveness in reflecting perceived fall risk.

Table 1: Correlation between fall hazard index and perceived fall risk using Spearman's rank.

Rank	Fall Hazard Index (0-1)	Fall Risk Perception	Rank
1	Uneven (0.92)	Uneven (5)	1
2	Debris (0.72)	Debris (5)	1
3	Slippery (0.06)	Slippery (3)	3

4. RESULT

The mean difference in the refined fall hazard index, integrated with EDA data, demonstrated a significant correlation with self-reported fall risk perception (average correlation coefficient = 0.82, $p < 0.01$). However, the correlation between the IMU-only fall hazard index and perceived fall risk was lower, with a correlation coefficient of 0.60 ($p < 0.01$). This discrepancy can be attributed to the limitations of relying solely on physical movement monitoring for fall risk assessment. Natural variations in arm movements during normal walking introduce abnormal patterns of wrist-worn IMU data, making it challenging to distinguish between normal walking and STF hazard exposure. In addition, even when abnormal movements occur due to hazard exposure, individuals may perceive lower fall risk if they anticipate the hazard and adjust their balance accordingly.

To further investigate this, a subgroup correlation analysis was conducted by dividing subjects into older adults (>60 years, n = 18) and young-middle-aged adults (<60 years, n = 42). The results revealed that the older adult group showed similar correlation coefficients for both the IMU-based, and the refined fall hazard indices (see Table 2). This difference in the benefit of EDA data between groups can be explained by the fact that older adults tend to have slower, more consistent arm movements during normal walking, reducing the likelihood of false positives. Furthermore, older adults are more likely to immediately perceive hazard due to higher sensitivity to physical disturbances. In contrast, the young-middle-aged group showed a significant improvement in correlation when EDA data was integrated (see Table 2). This finding is likely due to their greater variability in arm movements during normal walking, which complicates fall risk assessment using IMU data alone. Moreover, younger individuals often possess greater balance recovery abilities, leading them to underestimate fall risk even when abnormal physical movements are present. Thus, by incorporating EDA data, which captures physiological arousal triggered by stressful stimuli such as hazard exposure, the limitations of IMU-based fall risk assessment can be mitigated. This integration enhances the model's ability to accurately identify STF hazard exposures, leading to a more precise assessment of fall risk across diverse populations.

Table 2: Spearman's rank correlation between fall hazard index and self-reported fall risk by group.

Subjects (n)	Rank Correlation	
	IMU	IMU + EDA
Young-Middle (42)	0.51	0.86
Older (18)	0.81	0.81
All (60)	0.60	0.82

5. CONCLUSIONS

In this study, the authors demonstrate that the correlation between IMU-based fall risk assessment and fall risk perception varies, influenced by physical factors such as natural body movements and physical ability. These variations can affect the reliability of fall risk assessments from the perspective of end-users, potentially limiting the effectiveness of personalized interventions. To address these limitations, the authors propose an approach that integrates EDA data with the IMU-based fall hazard index to enhance the accuracy of fall risk assessment. This integration resulted in a stronger correlation with self-reported fall risk, achieving an average correlation coefficient of 0.82. Interestingly, the impact of this integration varied by age group. For older adults, their hazard perception closely matched physical responses. In contrast, young-middle-aged adults benefited from EDA integration, which captured perceptual variability not reflected in IMU data alone. This indicates that incorporating physiological arousal monitoring effectively improves the model's ability to reflect perceived fall risk, particularly when IMU data alone may be insufficient due to natural movement variability or differences in hazard perception.

Furthermore, by monitoring both physical and physiological responses from the wrist, this method offers a practical solution for large-scale implementation. Utilizing a single wearable wristband sensor that combines IMU and EDA technologies, the approach can be integrated into existing smartwatch platforms. This makes it feasible to implement in diverse settings, including construction sites, where workers are frequently exposed to environmental fall hazards, physical fatigue, and distraction. The proposed method can assist in identifying high-risk workers and enabling timely interventions to reduce fall incidents and improve overall safety in construction.

ACKNOWLEDGMENTS

The study described in this paper was supported by Liberty Mutual Insurance, Risk Control Services. Any opinions, findings, conclusions, or recommendations expressed in this paper are those of the authors and do not necessarily reflect the views of Liberty Mutual Insurance.

REFERENCES

Albert, M. V., Kording, K., Herrmann, M., and Jayaraman, A. 2012. Fall Classification by Machine Learning Using Mobile Phones. *PLoS ONE*, 7(5): e36556.

Antwi-Afari, M. F., and Li, H. 2018. Fall risk assessment of construction workers based on biomechanical gait stability parameters using wearable insole pressure system. *Advanced Engineering Informatics,* Elsevier, 38: 683–694.

Centers for Disease Control and Prevention, Number of Injuries and Associated Costs. https://wisqars.cdc.gov/cost/, 2022 (accessed February 7, 2025).

Sohn, J., Lee, H., Lee, G., Jacobs. J., and Lee, S. 2024. Feasibility of Applying a Wearable Electrodermal Activity Sensor for Individual Fall Risk Assessment. *International Conference on Computing in Civil Engineering.* ASCE, Pittsburgh, Pennsylvania, USA.

Karel, J. M. H., Senden, R., Janssen, J. E. M., Savelberg, H. H. C. M., Grimm, B., Heyligers, I. C., Peeters, R., and Meijer, K. 2010. Towards unobtrusive in vivo monitoring of patients prone to falling. *Annual International Conference of the IEEE Engineering in Medicine and Biology Society.* IEEE, Glasgow, Scotland, United Kingdom, 5018–5021.

Lee, H., Lee, G., Lee, S., and Ahn, C. R. 2022. Assessing exposure to slip, trip, and fall hazards based on abnormal gait patterns predicted from confidence interval estimation. *Automation in Construction*, Elsevier, 139: 104253.

Lee, J. K., Robinovitch, S. N., and Park, E. J. 2015. Inertial Sensing-Based Pre-Impact Detection of Falls Involving Near-Fall Scenarios. *IEEE Transactions on Neural Systems and Rehabilitation Engineering.* IEEE, 23 (2): 258–266.

Mao, A., Ma, X., He, Y., and Luo, J. 2017. Highly Portable, Sensor-Based System for Human Fall Monitoring. *Sensors,* 17 (9): 2096.

Okunola, A., Akanmu, A., and Jebelli, H. 2024. Fall risk assessment of active back-support exoskeleton-use for construction work using foot plantar pressure distribution. *Advanced Engineering Informatics.* Elsevier, 62: 102626.

Pang, I., Okubo, Y., Sturnieks, D., Lord, S. R., and Brodie, M. A. 2019. Detection of Near Falls Using Wearable Devices: A Systematic Review. *Journal of Geriatric Physical Therapy.* 42(1): 48–56.

Ramachandran, A., and Karuppiah, A. 2020. A Survey on Recent Advances in Wearable Fall Detection Systems. *BioMed Research International,* 2167160.

Sibley, K. M., Mochizuki, G., Lakhani, B., and McIlroy, W. E. 2014. Autonomic contributions in postural control: a review of the evidence. *Reviews in the Neurosciences*, 25(5): 687–697.

Skelton, D. A. 2001. Effects of physical activity on postural stability. *Age Ageing,* 30: 33–39.

Weiss, A., Shimkin, I., Giladi, N., and Hausdorff, J. M. 2010. Automated detection of near falls: algorithm development and preliminary results. *BMC Research Notes,* 3(1): 62.

Zhao, J., and Obonyo, E. 2020. Convolutional long short-term memory model for recognizing construction workers' postures from wearable inertial measurement units. *Advanced Engineering Informatics,* Elsevier, 46: 101177.